light for 2 h. Little decomposition was observed. The product was recovered by removing the heptane under reduced pressure. Of the total carbonyl content, 49% was ^{13}CO, as determined by mass spectroscopy. The relative amounts of $(C_6Et_6)Cr(^{13}CO)_3$ (11.9%), $(C_6Et_6)Cr(^{13}CO)_2(CO)$ (36.8%), $(C_6Et_6)Cr(^{13}CO)(CO)_2$ (38.1%), and $(C_6Et_6)Cr(CO)_3$ (13.2%) were calculated on the basis of stepwise equilibria.[60] The distribution of mass spectral peak intensities calculated for this statistical mixture matched the experimental data.

Variable-Temperature NMR Measurements. All variable-temperature $^{13}C\{^1H\}$ NMR spectra were recorded at 25.2 MHz in the Fourier transform mode on a Varian XL-100 spectrometer. All NMR samples were freeze–thaw degassed and sealed in 10-mm od sample tubes. Temperatures were measured with a copper-constantan thermocouple which was inserted, at coil height, into another 10-mm od sample tube containing an equal volume of the NMR solvent. Temperatures are considered to be accurate to ± 2 °C. Rates of exchange were measured in the temperature ranges of 223–273 K and 205–255 K for **2** and **3**, respectively.[62] The spin–lattice relaxation times (T_1) were obtained by the standard $(180°-\tau-90°-AT-PD)_n$ pulse sequence.[43b] Each T_1 determination was made from a linear least-squares fit of ten τ values. Pulse delays of $>5T_1$ were used.[63] The gated-decoupling technique[64] was used to determine the NOE's. Pulse delays of $\geq 10T_1$ were used in these experiments.[65] Sweep widths of 500 Hz and 8K Fourier transforms were used to ensure adequate digitization. Material labeled with ^{13}CO was used to substantially improve the signal/noise ratio obtained from the accumulation of two to ten transients.

Crystallography. Crystals suitable for X-ray analysis were obtained by slow crystallization from acetone (**1**), heptane (**2**, **3**), and heptane/benzene (**4**). The crystallographic data and details of data collection are reported in Table VI. Final atomic parameters for **1–4** are listed in Tables VII–X, respectively. The final difference map had no peaks greater than ±0.2, ±0.8, ±0.6, and ±0.6 eÅ^{-3} for **1–4**, respectively.

Acknowledgment. We thank the National Science Foundation (Grant CHE-8009670) for support of this work.

Supplementary Material Available: Final anisotropic thermal parameters with standard deviations for **1–4** (Tables XI–XIV) (4 pages). Ordering information is given on any current masthead page.

(60) The ratios of the stepwise formation constants used in these calculations were based on statistical arguments.[61] An isotope effect of unity was assumed for the exchange of free and complexed CO.

(61) Cotton, F. A.; Wilkinson, G. "Advanced Inorganic Chemistry", 3rd ed.; Interscience: New York, 1972; p 649.

(62) Experimental rate constants, in s^{-1} (temp, K), are 18 (223), 42 (232), 76 (237), 230 (246), 2150 (269), and 2750 (273) for **2** and are 2 (205), 40 (231), 77 (234), 185 (244), 350 (250), 600 (254), and 643 (256) for **3**.

(63) Harris, R. K.; Newman, R. H. *J. Magn. Reson.* **1976**, *24*, 449.

(64) Freeman, R.; Hill, H. D. W.; Kaptein, R. *J. Magn. Reson.* **1972**, *7*, 327.

(65) Canet, D. *J. Magn. Reson.* **1976**, *23*, 361.

Single-Crystal Polarized X-ray Absorption Spectroscopy. Observation and Theory for $(MoO_2S_2)^{2-}$

Frank W. Kutzler,† R. A. Scott,† Jeremy M. Berg,† Keith O. Hodgson,*† S. Doniach,‡ S. P. Cramer,§ and C. H. Chang§

Contribution from the Department of Chemistry and the Department of Applied Physics, Stanford University, Stanford, California 94305, and Exxon Research and Engineering Company, Linden, New Jersey 07036. *Received January 7, 1981*

Abstract: Linearly polarized synchrotron radiation has been used to investigate the orientation dependence of the K absorption edge of a single crystal of ammonium dithiomolybdate, the crystal structure of which is also reported herein. Following the collection of spectra with the polarization vector parallel to the oxygen–oxygen interatomic vector, the sulfur–sulfur vector, and the twofold rotation axis, self-consistent field Xα multiple scattered wave (SCF Xα MSW) calculations were done to interpret the observed orientation dependence. It is shown that this orientation dependence can be used to highlight the edge features which derive from molecular orbitals contributed to principally by the oxygen or the sulfur ligands. Anisotropy is also apparent in the extended X-ray absorption fine structure (EXAFS) spectra, which were recorded for orientations along the S–S and O–O interatomic vectors. It is thus demonstrated that polarized single-crystal X-ray absorption spectroscopy can provide orientationally selective information about the absorbing atom. It could, in principle, be used to deduce certain types of geometric information about the X-ray absorbing species.

Structural determination by X-ray diffraction requires long-range order in the sample. One of the primary advantages of the extended X-ray absorption fine structure (EXAFS) technique is that the absorbing atom need not be oriented in an extended array or lattice. Most of the X-ray absorption studies done heretofore have taken advantage of this freedom, measuring spectra for randomly oriented samples in solution, as powder, or as amorphous materials. The synchrotron radiation emitted from an electron storage ring is, however, linearly polarized in the horizontal plane and is well suited for use in absorption studies of oriented single crystals. The combination of oriented sample and polarized beam permits determination of the angular dependence of the absorption spectrum. The polarization effects can thus provide angularly selected structural information since the X-ray absorption spectrum contains information about the distances to, numbers of, and types of atoms surrounding the absorber.

In this paper we demonstrate the use of these effects in a study of the orientational dependence of the Mo K-edge absorption spectrum of ammonium dithiomolybdate, $(NH_4)_2MoO_2S_2$. The case of dithiomolybdate chosen for this study is particularly illustrative because the spectra from different orientations can be compared with those of molybdate and thiomolybdate which have been previously studied in experimental and theoretical detail.[1] In addition, the shape of the edges for different angles between the dithiomolybdate molecule and the polarization vector is interpreted by using molecular orbitals calculated from the self-consistent field Xα multiple scattered wave (SCF Xα MSW) formalism, which we have described earlier.[1] Also, we report here

†Department of Chemistry, Stanford University.
‡Department of Applied Physics, Stanford University.
§Exxon Research and Engineering Company.

(1) Kutzler, F. W.; Natoli, C. R.; Misemer, D. K.; Doniach, S.; Hodgson, K. O. *J. Chem. Phys.* **1980**, *73*, 3274.

0002-7863/81/1503-6083$01.25/0

the complete crystal structure determination of ammonium dithiomolybdate.

Recently, a polarization dependence of X-ray absorption has been observed in vanadium K-edge spectra of single crystals of vanadyl bis(acetylacetonate), $VO(C_5H_7O_2)_2$,[2a] in the Zn K edge of ZnF_2,[2b] and in studies of the selenium K edge and the tungsten L_{III} edge of a crystal of WSe_2.[3] Br_2 molecules adsorbed on graphite have also been examined in this manner.[4] Polarization effects have been shown to be useful in surface EXAFS[5,6] and angular resolved photoemission[7,8] studies as well.

The K-shell photoabsorption process involves the promotion of a 1s electron to a final state that is either an unoccupied valence state or an out-going continuum p wave. With use of the dipole approximation, the cross section of such an event, σ, is proportional to the dipole matrix element

$$\sigma \propto \sum_{\text{orient.}} \langle \psi_f | \vec{e} \cdot \vec{r} | \psi_i \rangle^2 = \sum_{\text{orient.}} \cos^2 \theta \, \langle \psi_f | \vec{r} | \psi_i \rangle^2 \qquad (1)$$

where the integral is over the initial and final state wave functions, $\vec{e}$ is the polarization direction, and θ is the angle between the polarization and dipole matrix operator vectors. Since the initial state in the cases we have studied is the fully symmetric 1s state of the central atom of the molecule, for a dipole-allowed process one of the components of the polarization vector must lie in the same representation as the final state.

In previous studies we have examined the K edges of four tetrahedral molecules, molybdate (MoO_4^{2-}), thiomolybdate (MoS_4^{2-}), chromate (CrO_4^{2-}),[1] and germanium tetrachloride ($GeCl_4$).[9] In the T_d point group, the x, y, and z components of the dipole operator all transform within the T_2 representation and therefore the spectrum is not orientation dependent. Similar results would be obtained in all cases of cubic symmetry.

However, the dithiomolybdate molecule has much lower symmetry, belonging to the C_{2v} point group, and a spectrum dependent on molecular orientation is expected to result. Wave functions in C_{2v} symmetry transform as either A_1, A_2, B_1, or B_2, and the dipole operator components of x, y, and z transform as B_1, B_2, and A_1, respectively. The transition probability is then

$$\sigma \propto \sum_{\text{orient.}} \{ \sum_{B_1 \text{ states}} \cos^2 X \, \langle 1s|x|\psi_f(B_1)\rangle^2 + \sum_{B_2 \text{ states}} \cos^2 Y \, \langle 1s|y|\psi_f(B_2)\rangle^2 + \sum_{A_1 \text{ states}} \cos^2 Z \, \langle 1s|z|\psi_f(A_1)\rangle^2 \} \qquad (2)$$

where X, Y, and Z are the angles between the polarization vector and the molecular axes.

In a powder or solution sample, the sum over all possible orientations results in an average value of one-third for the squared cosine of all three angles, yielding an averaged spectrum. On the other hand, if the absorber is a single crystal, the summation need include only the orientations within a single unit cell. For the dithiomolybdate crystal discussed here, the C_2 axes of all molecules in the unit cell are collinear with the crystallographic b axis, thereby simplifying the orientational averaging. Thus, the ammonium dithiomolybdate crystal is a good case for studying the anisotropy of absorption purely in the O–Mo–O plane, the S–Mo–S plane, or between them.

Experimental Section

Preparation of $(NH_4)_2MoO_2S_2$. The compound was prepared by a previously described method.[10] In 125 mL of distilled water, sodium molybdate, $Na_2MoO_4 \cdot 2H_2O$ (96.2 g, 0.40 mol), was dissolved and cooled to ice-water temperature. One hundred milliliters of concentrated ammonium hydroxide, NH_4OH (30%, Baker reagent grade), was cooled to ice-water temperature, and hydrogen sulfide (H_2S, 27.2 g, 0.80 mol, Scientific Gas Products) was added to the NH_4OH solution. This solution, when added to the molybdate solution, resulted in the immediate formation of fine orange crystals. After the mixture was left standing at ice-water temperature for 1 h, the precipitate was collected and washed with methanol. Single crystals of up to several millimeters were grown by storing the mother liquor at low temperatures for several days. Anal. Calcd for $(NH_4)_2MoO_2S_2$: Mo, 42.05; O, 14.03; S, 28.11; N, 12.28; H, 3.53. Found: Mo, 42.36; O, 13.87; S, 28.27; N, 12.14; H, 3.06.

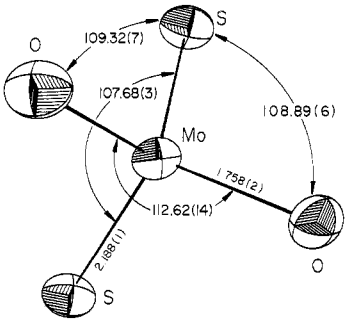

Figure 1. Drawing of a single dithiomolybdate ion, with the bond distances and angles as indicated. The thermal ellipsoids are plotted at the 50% probability level.

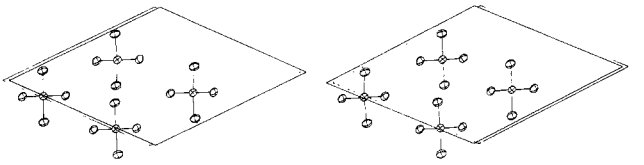

Figure 2. Stereoscopic packing diagram for $(NH_4)_2MoO_2S_2$ viewed down the b axis and with the a axis to the right of the lowest vertex. The Mo atoms occupy positions on the twofold axis. Ammonium cations have been omitted for clarity. The salient features are that each ion resides in the cell with the same orientation and that the O–O interatomic vectors and the S–S interatomic vectors form essentially right angles.

Crystallographic Determination. A Syntex $P2_1$ four-circle diffractometer using graphite-monochromatized Mo Kα radiation was employed for the structure determination. From 15 machine-centered reflections, taken from a rotation photograph, a monoclinic cell was chosen with the dimensions (in angstroms) a = 11.376 (3), b = 7.300 (2), and c = 10.923 (3), and β = 130.16 (2)°. A short data set was then collected, and the extinction condition $h + k = 2n$ was observed for all hkl. This pattern is compatible with the space groups $C2$, Cm, $C2/m$, Cc, and $C2/c$. The latter two groups possess the further extinction condition that $l = 2n$ for all $h0l$ present, a condition which was also observed, although comparatively weak exceptions were noted. Subsequent Patterson function analysis eliminated the possibility of the groups $C2$, Cm, and $C2/m$. Because the crystal diffracted quite intensely, it is reasonable to assume that the exceptions to the $h0l$ condition were due to Renninger spots.

The density was determined by the flotation method by using chloroform and bromoform, and the observed value of 2.16 g/cm^3 matches the value of 2.18 g/cm^3 calculated by using $Z = 4$. Tentatively, with the assumption of the space group $C2/c$, which has eight general positions, the Mo atoms were constrained to lie on the twofold axes. Successful refinement of the structure was taken as confirmation of $C2/c$ as the proper group. A similar assignment was made by Muller et al.[11] Lattice parameters were determined by least-squares refinement of 15 reflections chosen from the abbreviated data set. ω scans testing the mosaicity of the crystal gave narrow peaks, with full widths at half maximum of 0.2° or less. Data were collected in the quarter sphere $+h$, $+k$, $\pm l$, for 2θ values of 3–60°, and were then processed as described previously.[12,13] Rejection of all reflections weaker than three times their standard de-

(2) (a) Templeton, D. H.; Templeton, L. K. *Acta Crystallogr., Sect. A* **1980**, *A36*, 237. (b) Cox, A. D.; Beaumont, J. H. *Philos. Mag. [Part] B* **1980**, *1*, 126.
(3) Heald, S. M.; Stern, E. A. *Phys. Rev. B* **1977**, *16*, 5549.
(4) Heald, S. M.; Stern, E. A. *Phys. Rev. B* **1978**, *17*, 4069.
(5) Stohr, J.; Johansson, L.; Lindau, I.; Pianetta, P. *Phys. Rev. B* **1979**, *20*, 664.
(6) Citrin, P. H.; Eisenberger, P.; Hewitt, R. C. *Surf. Sci.* **1979**, *89*, 28.
(7) Stohr, J.; Apai, G.; Wehner, P. S.; McFeely, F. R.; Williams, R. S.; Shirley, D. A. *Phys. Rev. B* **1976**, *14*, 5144.
(8) Allyn, C. L.; Gustafsson, T.; Plummer, E. W. *Chem. Phys. Lett.* **1977**, *47*, 127.
(9) Natoli, C. R.; Kutzler, F. W.; Misemer, D. K.; Doniach, S. *Phys. Rev. A* **1980**, *22*, 1104.
(10) (a) Kruss, G. *Justus Liebigs Ann. Chem.* **1884**, *225*, 6. (b) Corleis, E. *Ibid.* **1886**, *232*, 254.
(11) Muller, V. A.; Diemann, E.; Baran, E. J. *Z. Anorg. Allg. Chem.* **1970**, *375*, 87.
(12) Bobrik, M. A.; Hodgson, K. O.; Holm, R. H. *Inorg. Chem.* **1977**, *16*, 1851.
(13) The structural determination used, along with local programs, the Structure Determination Package provided by Enraf-Nonius, Inc. Figures 1 and 2 were drawn by using ORTEP, and all calculations were carried out on a PDP 11/55 Computer.

Table I. Summary of Crystal Data

formula	$(NH_4)_2MoO_2S_2$
a, Å	11.376 (3)
b, Å	7.300 (2)
c, Å	10.923 (3)
β, deg	130.16 (2)
V, Å^3	693.28
Z	4
d_{calcd} (d_{obsd}), g/cm^3	2.186 (2.16)[a]
space group	$C2/c(C_{2h}^6)$
cryst dimens, mm	0.20 × 0.30 × 0.30[b]
radiation[c]	Mo (λ(Kα) 0.710 69 A)
ab coeff (μ), cm^{-1}	23.45
max transmissn coeff	0.8696
min transmissn coeff	0.6674
takeoff angle, deg	3.0
scan speed, deg min^{-1}	1–29.3 (θ–2θ scan)
scan range, deg	0.8 below $K\alpha_1$ to 0.8 above $K\alpha_2$
bkgd counts	bkgd/scan time = 0.25
2θ limits, deg	3–60
unique data ($F_o^2 > 3\sigma(F_o^2)$)	797
error in observn of unit wt	1.77
R, %	3.2
R_w, %	5.0

[a] Determined by flotation in chloroform/bromoform. [b] Approximate, irregularly shaped. [c] Monochromated from mosaic graphite.

viation left 797 reflections to be used in the refinement of the structure.

The locations of the Mo and S atoms were determined by the Patterson function, and difference Fourier analysis elicited the positions of the O, N, and two of the H atoms. The other two hydrogenic positions were calculated by assuming tetrahedral geometry about the nitrogen. All atomic positions and thermal parameters, except those of the calculated hydrogen atoms, were refined by full-matrix least squares. The atomic scattering factors were taken from standard tables, and the weighted and unweighted R factors, calculated from $R = \sum||F_o| - |F_c||/\sum|F_o|$ and $R_w = [\sum w(|F_o| - |F_c|)^2/\sum w|F_o|^2]^{1/2}$, refined to 3.2 and 5.0%, respectively. The estimated standard deviation (ESD) in an observation of unit weight, obtained from the expression esd = $[\sum w(|F_o| - |F_c|)^2/(N_o - N_v)]^{1/2}$ where N_o is the number of observations and N_v is the number of refined variables, was 1.77. The largest parameter shift in the final least-squares cycle was 0.09 times the estimated standard deviation, and the highest peak in the final difference Fourier map was about 0.12 times the height of a nitrogen atom peak.

A summary of crystallographic information is given in Table I, and the atomic positions are given in Table II. Figure 1 displays a single dithiomolybdate ion, while Figure 2 shows the packing of the four dithiomolybdate ions within a unit cell. (The ammonium ions have been omitted for clarity.)

X-ray Absorption Measurements. X-ray absorption measurements were carried out at the Stanford Synchrotron Radiation Laboratory (SSRL). Since the crystal used for diffraction studies was inconveniently small for absorption measurements, a larger specimen, approximately 3.5 × 1.5 × 0.7 mm, was mounted on a fiber, and an orientation matrix was determined by using a CAD4 diffractometer. This matrix yielded lattice parameters essentially identical with those obtained from the crystal used for the structure determination.

Positioning of the crystal with respect to the polarization vector was accomplished through the orientation matrix, the CAD4 positioning mechanism, and the Enraf-Nonius CAD4 software.[14] Absorption spectra of the crystal were collected in four orientations. The first was with the S–S interatomic vector parallel to the polarization vector. This sets X in eq 2 to 0° and Y and Z to 90°, selecting only final-state wave functions of B_1 symmetry. The second orientation was obtained by a 90° rotation about the twofold axis, aligning the O–O vector with the polarization vector, thereby selecting 1s to B_2 transitions. A third, mixed orientation spectrum midway between the first two orientations was measured, and the fourth orientation, which selected only A_1 final states, aligned the z axis with the polarization vector. The X-ray beam from the electron storage ring was monochromated by a two-crystal monochromator by using Si[220] crystals. The incident and transmitted beam intensity was measured with argon-filled ion chambers. After the first chamber, the beam was defined by a 0.75-mm diameter diffractometer collimator, in order to ensure that only X-rays passing through the crystal would reach the second chamber.

The experimental spectra presented here were averaged from three independent scans. A given point for each spectrum was integrated for 1–2 s, and the monochromator stepped in intervals of approximately 1 eV. The data were processed as described previously[15] by using the first inflection point on the absorption edge of a Mo foil at 20 003.9 eV for calibration.

Calculations

Since the basis of the SCF Xα MSW method has been extensively discussed elsewhere,[16,17] only an abbreviated overview is offered here. The crux of the approximation is the division of the molecule into three volumes. The first type is a set of spheres centered on nuclei, and is collectively labeled region I. Region III is the volume outside an "outer sphere" which encloses all the atomic spheres. The remaining region between the atomic spheres and the outer sphere is known as the interstitial, intersphere, or constant potential region, or as region II.

Our initial potential was constructed for each atom by using the Clementi–Roetti wave functions for neutral atoms.[18] These atomic potentials were superimposed, and a set of atomic sphere boundaries was established as discussed below. The potential within each atomic sphere and outside the outer sphere was radially averaged, allowing the separation of the radial and angular parts of the Schrödinger equation. The charge density in the computationally difficult intersphere region was averaged, and the entire region was assigned a single, constant potential.

A numerically integrated solution, to within a scaling constant, was calculated for each of the atomic spheres (region I), and for the outer sphere (region III). The solution for region II can be expressed as a linear combination of spherical Bessel and Neumann functions, owing to the constant potential approximation. Matching these wave functions and their first derivatives at the boundaries adjoining region II with regions I and III leads to a set of secular equations, which determines the values of the scaling constants of each individual component of the total wave function. The determinant of these equations is a function of energy, and eigenenergies were isolated by locating the zeroes of the determinant. From the eigenenergies, the total bound state wave functions were calculated. For positive energies, the wave functions are no longer required to vanish at infinity and, as a result, a wave function can be computed for continuous energies. Input parameters for this calculation are listed in Table III. Our experience[9] has suggested that the most reliable manner of determining the atomic sphere radii is a method proposed by Norman.[19] In this prescription, the initial superimposed charge density is integrated outward from each nucleus until the charge of the enclosed electron density equals the charge of the nucleus. This method defines a set of radii ratios which generally overlap to a large degree. These ratios can then be scaled to achieve any degree of overlap, and Norman has suggested that 25–30% is a suitable choice.[19] In our studies of molybdate,[1] we showed that a small amount of overlap, about 10% or less, has only a minor effect on both the energy levels and the calculated K edge. On the other hand, larger overlaps of 30% had a large, and not necessarily favorable, effect on the predicted vs. experimental K edges of molybdate and thiomolybdate. Therefore, we have used the Norman procedure to determine the radii ratios but have allowed the Mo and S to just touch, which leads to a Mo–O overlap of about 4.5%. Slater exchange (α) parameters were taken from Schwarz[20] for O and S, and a value was extrapolated for Mo. A simple average of atomic values was used for the intersphere and outer-sphere regions.

The initial potential was searched for eigenstates, and these states were populated to bring the total charge of the complex

(14) Enraf-Nonius CAD4 Operations Manual; Enraf-Nonius: Delft, Holland, 1977.

(15) Cramer, S. P. Ph.D. Thesis, Stanford University, Stanford, California, 1978.

(16) (a) Johnson, K. H. *Adv. Quantum Chem.* **1973**, *7*, 143. (b) *Annu. Rev. Phys. Chem.* **1975**, *26*, 39.

(17) (a) Dill, D.; Dehmer, J. L. *J. Chem. Phys.* **1974**, *61*, 692. (b) Siegel, J.; Dill, D.; Dehmer, J. L. *Ibid.* **1976**, *64*, 3204.

(18) Clementi, E.; Roetti, C. *At. Data Nucl. Data Tables* **1974**, *14*, 177.

(19) Norman, J. C., Jr. *Mol. Phys.* **1976**, *31*, 1191.

(20) Schwarz, K. *Phys. Rev. B* **1972**, *5*, 2466.

Table II. Positional and Thermal Parameters for $(NH_4)_2MoO_2S_2$

atom	x	y	z	β_{11}[a]	β_{22}	β_{33}	β_{12}	β_{13}	β_{23}
Mo	0.00000	0.33482 (4)	0.25000	0.00735 (4)	0.00659 (5)	0.00622 (3)	0.0000 (0)	0.00830 (4)	0.0000 (0)
S	0.1826 (1)	0.5117 (1)	0.44357 (8)	0.00947 (9)	0.0100 (1)	0.00817 (8)	−0.0026 (2)	0.0085 (1)	−0.0033 (1)
O	0.0729 (3)	0.2013 (3)	0.1783 (2)	0.0097 (3)	0.0103 (3)	0.0084 (2)	0.0019 (5)	0.0114 (3)	−0.0032 (4)
N	0.3868 (3)	0.3151 (3)	0.3382 (3)	0.0109 (4)	0.0102 (4)	0.0099 (2)	−0.0006 (5)	0.0141 (4)	−0.0018 (5)

	x	y	z	B, Å²		x	y	z	B, Å²
H1	0.725 (6)	0.293 (7)	0.215 (5)	4.3 (11)	H3[c]	0.055	0.207	0.527	9.0
H2	0.390 (4)	0.560 (6)	0.821 (4)	3.0 (9)	H4[c]	0.446	0.243	0.312	9.0

[a] The form of the anisotropic thermal ellipsoid is $\exp[-(\beta_{11}h^2 + \beta_{22}k^2 + \beta_{33}l^2 + \beta_{12}hk + \beta_{13}hl + \beta_{23}kl)]$. [b] Estimated standard deviations in parentheses. [c] The following parameters were calculated by assuming tetrahedral geometry about the N atom and were not refined.

Table III. Input Parameters for SCF Xα MSW Calculation

sphere	max L[a]	x	y	z	R[b]	exchange[c]
Mo	4 (5)	0.000	0.000	0.000	1.030	0.70342
S1	2 (3)	1.818	0.000	1.203	1.147	0.72426
S2	2 (3)	−1.818	0.000	1.203	1.147	0.72426
O1	1 (2)	0.000	1.433	−1.022	0.807	0.74367
O2	1 (2)	0.000	−1.433	−1.022	0.807	0.74367
outer sphere	4 (10)	0.000	0.000	0.000	3.330	0.72790
intersphere						0.72790

[a] Maximum angular momentum used in the basis functions for bound states and continuum (in parentheses). For further details, see ref 1. [b] Radii ratios chosen by Norman's procedure (see ref 19), with Mo and S spheres touching and Mo and O overlapping by about 4.5%. [c] See ref 20.

to 2−. This potential was iterated to self-consistency, at which time the eigenvalues were changing by less than 0.001 Ry/iteration. The electron population was then altered, and the system was allowed to relax back to self-consistency, producing a set of "excited states" in which the electron occupied a valence orbital and the "ionized state" in which the 1s electron was removed. In molybdate and thiomolybdate, the use of different orbitals for electrons with different spins, the so-called spin-unrestricted calculation, was found to have negligible influence on the calculated edges,[1] so only spin-restricted calculations were done for dithiomolybdate. The positions of the bound-state features with respect to the ionization threshold were obtained by comparison of the total statistical energies of the excited and ionized states. Transition matrix elements were calculated in two ways. The simpler approach was to use wave functions as they exist in the ground-state potential. This method ignores the relaxation process, which necessarily accompanies the transition. The second method is to calculate the matrix element with the 1s orbital as formed in the ground state but to use final-state wave functions as calculated in the corresponding excited-state potential. This method accounts for relaxation, but the spectator orbitals, for which the electron occupancy remains constant, are no longer orthonormal with their counterparts in the ground state, since they have been calculated by using different Hamiltonians. A complete matrix element calculation would involve the full Slater determinant, but the active electron approximation was used, which employs only the initial and final eigenfunctions in the matrix element calculation. The values from both methods gave results to within about 5% of each other, and those from the excited-state potentials were used in the composition of the K edges.

The continuum wave functions were calculated in a potential field which had been allowed to relax to self-consistency in the presence of the 1s core hole. This potential was modified by the Hedin-Lundqvist correction for local many-body effects.[21]

Finally, the absorption cross sections for both the bound and the continuum wave functions were convolved with a Lorentzian function of energy with a full width at half maximum (fwhm) of 7.6 eV. This accounts for the dual effects of the 1s lifetime broadening and the broadening due to the divergence of the beam through the monochromator. The form of the broadening function by the lifetime effect is nearly Lorentzian, and the fwhm has been calculated by Kostroun et al. to be about 4.6 eV.[22] A Gaussian with a fwhm of 4.6 eV was used to account for the synchrotron divergence.[23] The convolution of a Gaussian and a Lorentzian of these widths results in a function with a fwhm of about 7.6 eV.

Results and Discussion

Each unit cell, displayed in Figure 2, contains four dithiomolybdate ions, each positioned on a twofold rotation axis. The ion has a Mo–O bond length of 1.758 (2) Å and a Mo–S bond length of 2.188 (1) Å (see Figure 1). The coordination about the Mo is very nearly tetrahedral, with angles of 107.68 (3)° for S–Mo–S, 112.62 (14)° for O–Mo–O, and 108.89 (6) and 109.32 (7)° for O–Mo–S. For the purposes of the absorption edge interpretation, three features are of primary importance. First, the twofold rotation axis guarantees that both the O–O and the S–S interatomic vectors are perpendicular to the twofold axis. Second, the O–O and S–S interatomic vectors are very nearly perpendicular, forming an angle of about 89.1°. Finally, all four dithiomolybdate ions are situated in the unit cell with the same orientation. Hence, the sum over the orientations in eq 1 and 2 can be reduced to that of a single molecule. For convenience, we have defined the molecular coordinates such that the z axis and the twofold rotation axis are collinear and, furthermore, such that the sulfurs lie in the x–z and the oxygens in the y–z planes. An outgoing p wave of B_1 symmetry, which is oriented along the x axis, will be most influenced by the potential barrier of the sulfur atoms, whereas a B_2 outgoing wave is predominantly affected by the oxygens. An A_1 wave experiences the effects of both sulfur and oxygen.

Comparisons of the Lorentzian-broadened calculations with the experimental spectra are displayed in Figure 3a–c, in which the solid lines are experimentally obtained, and the dotted curves are the total calculated values. The lower solid lines represent the contributions of the bound and continuum portions of the calculations. The residual relativistic error following the use of first-order perturbation corrections is about 20–30 eV. Since our primary interest involves the relative energies of the spectral features, the energies of the calculated curves have been positioned to align the lowest energy feature. Also, the overall heights of the experimental data have been scaled to match those of the calculated spectra.

(21) (a) Hedin, L.; Lundqvist, B. I. *J. Phys. C* **1971**, *4*, 2064. (b) von Barth, U.; Hedin, L. *Ibid.* **1972**, *5*, 1629. (c) Gunnarson, O.; Lundqvist, B. I. *Phys. Rev. B* **1976**, *13*, 4274.

(22) Kostroun, V. O.; Chen, M. H.; Crasemann, B. *Phys. Rev. A* **1971**, *3*, 533.

(23) Kincaid, B. Ph.D. Thesis, Stanford University, Stanford, California, 1975.

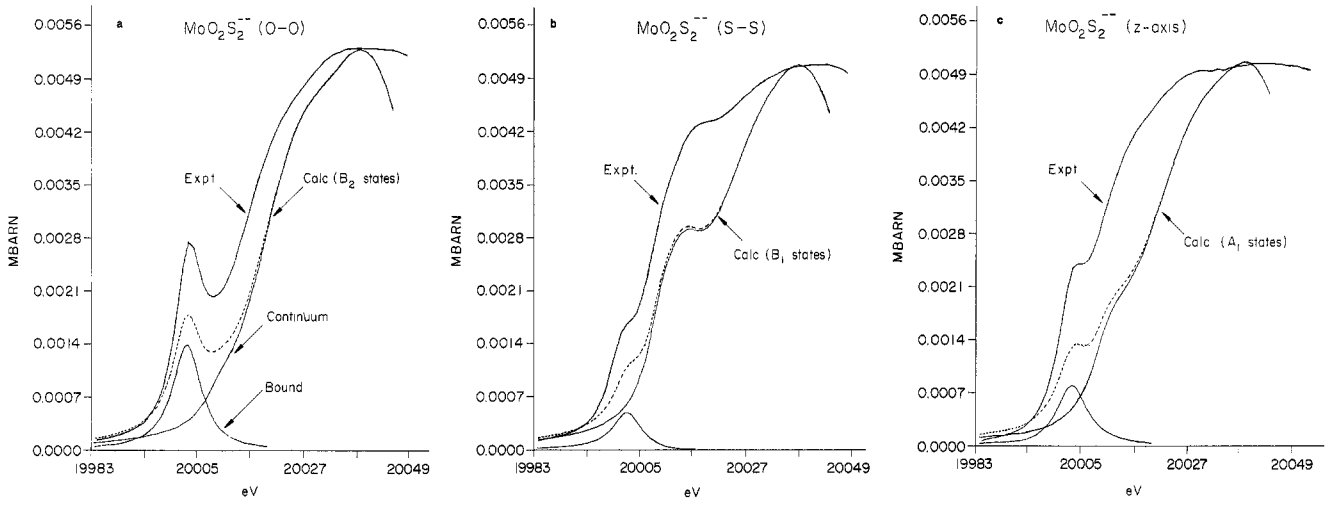

Figure 3. Experimental spectra (upper solid lines) obtained from three different crystal orientations. The dashed lines are the spectra predicted by the calculations, in which the energies have been adjusted as noted in the text. The lower solid lines depict the bound and continuum contributions to the calculated spectra: (a) The spectrum with the O–O interatomic vector parallel to the polarization vector and the result of transition cross sections to final states of B_2 symmetry; (b) The spectrum with the S–S vector collinear with the polarization vector and with B_1 final states; (c) The spectrum with the molecular z axis (two fold axis) parallel to the polarization vector and with A_1 final states.

Examination of the figures indicates that the calculations are successful in reproducing the general form of the spectra. Experimental peaks and shoulders are reproduced by calculated features to within a few electron volts of the observed positions. The most poorly represented region is at higher energy, where the calculated curves fall off too quickly. We have found this to be a general feature in all the calculations that we have done thus far.[1] Although the truncation of the angular momentum (L) basis set will eventually lead to distortion at high energies, it is unlikely that this truncation is at fault here, since most of the peak behavior is provided by the lowest L partial waves. A more likely explanation lies in a deficient representation of the energy dependence of the potential at these energies, and that multielectron events, which are invisible to our one-electron scheme, are providing the system with absorption channels for which we cannot account.

Results for each of the representations are now discussed separately. Figure 3a shows the spectrum obtained when the O–O vector is collinear with the polarization vector. This calculation involves the B_2 final state, since the y component of the dipole operator transforms as B_2. Within this representation we find one bound state with a large oscillator strength about 5.4 eV below the ionization threshold. This state has 36% of the charge within the Mo sphere, mostly in the $L = 2$ basis function, and 9% in each of the two oxygens. Only about 4% of the total charge resides in the sulfur atoms. The remainder of the charge was either outside the outer sphere or in the intersphere region. The presence of this state shows up clearly at about 20 004 eV. The energy separation between the bound state and the principal continuum peak is calculated to be 38 eV, as opposed to 35 eV in the experiment. These values are precisely the same as previously obtained in the calculation of molybdate.[1] Like the earlier molybdate results, the calculated bound state appears weaker relative to the continuum cross sections than does the experimental shoulder.

Figure 3b shows the spectrum with the S–S vector in alignment with the polarization vector. The pertinent representation in this calculation is B_1. The B_1 bound state, which has a weaker transition probability than does the B_2 state, lies about 6.8 eV below ionization. The wave function is, like the B_2 state, primarily of Mo d character, with 37% of the charge residing inside the Mo sphere and with most of the remainder (14%) in each of the two sulfur atoms. The weakness of the oscillator strength of this B_1 state is reflected in the disappearance of the clear low-energy feature seen in the B_2 spectrum, with only an unresolved shoulder being seen. The experimental spectrum corresponding to the B_1 state (S–S orientation) also shows a shoulder at higher energies. This higher energy shoulder is found in the calculations at about 20 015 eV and is the result of a continuum resonance rather than a second bound-state transition. The energy separation between the two shoulders is experimentally 15 eV, compared to the calculated value of ca. 12 eV. The energy separation between the low-energy shoulder and the overall maximum is 35 and 40 eV in the calculation and experiment, respectively. It is interesting that while the ratio of the strengths of the two shoulders is about the same in the calculation as in the experiment, the strengths of both features in the calculation are too weak when compared to the highest maximum.

Figure 3c shows the spectrum obtained with the polarization along the molecular z axis. This orientation is in several ways an average of the two preceding orientations, both in theory and experiment. The low-energy feature in this orientation is neither as distinct as in the O–O orientation nor as subtle as in the S–S orientation. The quality of the data for this orientation is poorer than for the other orientations, since the morphology of the crystal was such that this spectrum was taken through the long axis, and hence the amount of transmitted beam was quite small. It is uncertain to what extent the data can be trusted, and perhaps for this reason the agreement of the calculations with the experiment is less favorable here than for the previous two orientations. We found three bound states in the A_1 representation, ranging from 6.8 to 7.4 eV below the continuum, although one of these states contained nearly 80% of the oscillator strength. The nature of the lower two states is primarily Mo d, with nearly equal mixtures of oxygen and sulfur p character.[24] The highest of these states resembles a Mo 5p state, but a large amount of charge is resident in the intersphere region and outside the outer-sphere boundary. These bound states appear collectively as the peak at about 20 004 eV. At about 20 015 eV in the calculation there is a second shoulder which has no apparent counterpart in the experimental spectrum. This is probably a consequence of the thickness of the crystal in this orientation.

Apart from the comparison of experimental and calculated spectra, it is interesting to compare the dithiomolybdate spectra with the "pure" counterparts of molybdate and thiomolybdate. Figure 4 depicts the edge and EXAFS of two orientations of the dithiomolybdate crystal, one in which the S–S vector is parallel to the polarization vector, and the other which positions the O–O vector in approximate alignment. Figure 5 shows the K absorption

(24) The behavior of these three states is somewhat enigmatic, in that the composition and oscillator strengths change somewhat depending on whether the electron configuration is a ground or excited state. The total oscillator strength of all three orbitals remains nearly unchanged, however, and this ambiguity makes little difference in the calculated edge.

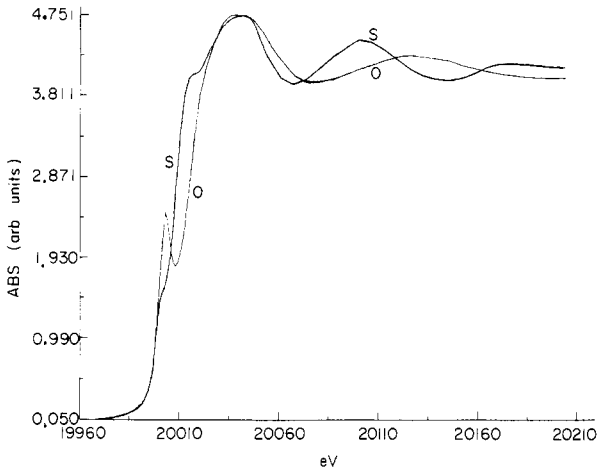

Figure 4. Edge and EXAFS spectra for two orientations of ammonium dithiomolybdate. The spectrum marked S was taken with the S–S interatomic axis essentially parallel to the polarization vector and the spectrum labeled O was at 90° to this orientation. The O spectrum contains a small percentage of z axis contribution (roughly 10%), since this spectrum was approximated before the crystal structure was known.

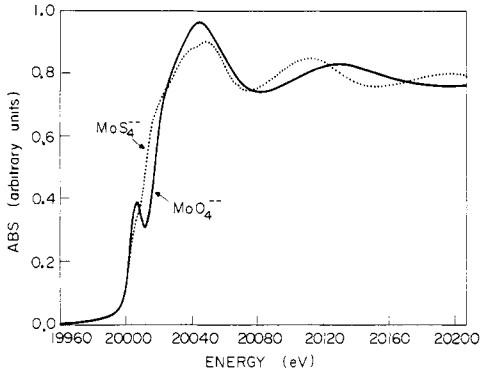

Figure 5. Edge and EXAFS spectra of molybdate (solid line) and thiomolybdate (dashed line), to be compared with the O–O and S–S orientations of dithiomolybdate, given in Figure 4.

spectra for molybdate and thiomolybdate. It is apparent that both the edge and EXAFS of molybdate are quite similar to the spectrum for the O–O orientation of dithiomolybdate. Likewise, great similarity exists between the S–S orientation and the thiomolybdate spectrum. These figures clearly demonstrate that proper orientation of the crystal can successfully resolve the spectrum produced by an anisotropic ligand configuration. The different orientations of dithiomolybdate also demonstrate the general observation that second-row ligands induce broader, less resolved edges than do the first-row ligands (as in the series of vanadium halides, VF_3, VCl_3, and VBr_3[25]).

Although in this study the EXAFS region of the dithiomolybdate spectrum has not been quantitatively analyzed, we can say that the observed effects are qualitatively as expected. The contribution of a given scatterer to the EXAFS is proportional to 3 $\cos^2\theta$, where θ is the angle between the polarization vector and the position vector of the scatterer. The Mo–O and Mo–S distances in dithiomolybdate are within 0.02 Å of the corresponding distances in molybdate and thiomolybdate. It is therefore not surprising that the EXAFS of the dithiomolybdate crystal in certain orientations resembles the EXAFS of molybdate or thiomolybdate. Aligning the polarization vector parallel to the O–O interatomic vector makes the polarization vector perpendicular to the Mo–S vectors, while the angle with the Mo–O vectors is 33.7°. Thus, in this orientation we should see no Mo–S contribution to the EXAFS, and a Mo–O component with an amplitude (2/4) × 3 $\cos^2$ (33.7°) = 1.04 times that of molybdate. (A factor of exactly 1.00 would result if the dithiomolybdate bond angles were precisely tetrahedral.) The converse is expected for the orientation along the S–S vector. As can be seen by the comparison of Figures 4 and 5, the EXAFS is qualitatively as predicted, but a quantitative comparison must await better data over a wider energy range.

(25) Tullius, T. D. Ph.D. Thesis, Stanford University, Stanford, California, 1978.

Conclusions

The current study has demonstrated that dramatic anisotropy can occur in the K absorption edge of molybdenum compounds with the appropriate molecular and crystalline symmetry. In the specific case of ammonium dithiomolybdate, the orientation in which the O–O axis is collinear with the polarization vector yields a spectrum that is very similar to the spectrum obtained for molybdate, while the S–S orientation spectrum strongly resembles thiomolybdate. As expected, in the intermediate cases, an average spectrum is obtained. All of these effects have been interpreted here by using SCF Xα MSW calculations.

Oriented single-crystal X-ray absorption studies may be of particular value in the structural characterization of many types of biological metal centers, in which the metal ligation is often anisotropic. For example, such experiments would be useful when one orientation involves first-row ligands and a perpendicular orientation is directed toward heavier atoms. In such cases one would expect clear changes in the shape and position of the absorption edge. One particularly exciting prospect is to use the sharp bound-state transition associated with the terminal oxo group to obtain the orientation of the oxomolybdenum bond(s) with respect to other prosthetic groups within molybdenum enzyme crystals.

In previous work, one of the principal limitations of bioinorganic EXAFS studies has been the lack of geometrical information about ligands in the metal coordination sphere. Single-crystal EXAFS studies offer the possibility of determining the angular orientation of a particular absorber–scatterer axis within a crystal. Of course, this determination is limited to within $\pm\pi$ radians, since the outgoing photoelectrons probe along both directions of the polarization vector simultaneously. Furthermore, for unambiguous work one requires a unit cell with only a single type and orientation of the X-ray absorbing atoms of interest. Still, there are undoubtedly many cases where the combination of oriented EXAFS data and other chemical information will lead to significant advances in structural understanding.

In short, single-crystal edge and EXAFS studies show great promise in providing even more information than do the classical randomly oriented experiments and provide an avenue through which geometrical information can be obtained from X-ray absorption, a potential which has yet to be exploited.

Acknowledgment. This work was supported by the National Science Foundation through Grant PCM 79-04915 and the Center for Materials Research at Stanford University. R.A.S. is the recipient of an NIH postdoctral fellowship (Grant 3-F32-HL06047-01S1). Synchrotron radiation beam time was provided by the Stanford Synchrotron Radiation Laboratory which is supported by the National Science Foundation through Grant DMR-77-27489, in cooperation with the Stanford Linear Accelerator Center and the United States Department of Energy.

Supplementary Material Available: A listing of final structure factors (Table IV) (4 pages). Ordering information is given on any current masthead page.